2021 43rd Annual International Conference of the
IEEE Engineering in Medicine & Biology Society (EMBC)
Oct 31 - Nov 4, 2021. Virtual Conference

Multi-session Analysis of Movement Variability While Reaching in a Virtual Environment*

Paul VanGilder, Kris Phataraphruk, Christopher A Buneo

Abstract— **The acquisition of neurophysiological data during awake, behaving animal experiments typically involves experimental sessions lasting several days to weeks. Therefore, it is important to understand natural fluctuations in behavioral performance over such periods. Here we quantified patterns of movement variability for reaches performed by two monkeys across five daily experimental sessions. The monkeys were trained to move in an immersive virtual reality (VR) environment that was designed to resemble the experimental room. Visual feedback of the limb was provided using VR avatar arms that were controlled through a reflective marker-based motion capture system. Additionally, tactile cues were provided in the form of physical reach targets. Spatial variability was characterized at early (peak acceleration) and late (movement endpoint) kinematic landmarks. We found that the magnitude of variability was generally larger at peak acceleration than at the endpoint but was relatively consistent across days and within animals. The spatial characteristics of variability were also generally highly consistent at peak acceleration both within and between animals but were noticeably less so at the endpoint. The results highlight the benefits of using early kinematic landmarks such as peak acceleration for quantifying movement variability in reaching studies involving animals.**

I. Introduction

Reaching movements are prone to variability, even under identical task and sensory conditions. This variability is attributed in part to noise in the nervous system, which can manifest during the sensing, planning, and execution stages of sensorimotor processing [1]. Neural noise may influence estimates of limb state (i.e., position and velocity) arising from visual and proprioceptive feedback [2], which in turn influences the movement planning process [3] and results in variability in movement direction, amplitude, and speed [4]. It is known that the accuracy and precision of limb state estimates can be improved by combining multiple sources of sensory information (vision, proprioception, taction) through a process called multisensory integration [5]. Behavioral studies suggest that this integration process can be described within a Bayesian inference framework, i.e., sensory cues are weighted based on their relative reliability (which can change depending on sensory or motor context [6]–[8]) and combined with prior knowledge to form a single limb state estimate. The neural mechanisms underlying this phenomenon are still largely unclear but are important for understanding both basic sensorimotor processing and for the development of closed-loop neural prostheses.

To facilitate study of the neural mechanisms of sensorimotor integration, we recently developed a system that pairs a realistic virtual reality (VR) environment with real-time motion tracking of the limb [9]. More specifically, the VR environment allows for systematic manipulation of arm visual feedback and thus can be used to investigate the neural correlates of visual, proprioceptive, and tactile integration during the planning and execution of arm movements. Since acquiring neural data during such investigations typically involves experimental sessions lasting several days to weeks, it is important to understand natural fluctuations in behavioral performance over such time frames. However, although reaching variability has been well characterized in multiple contexts (e.g., [4], [10]), the consistency of variability metrics over multiple experimental sessions in a virtual environment has not to our knowledge been previously addressed. As a result, we quantified patterns of movement variability for reaches performed across multiple experimental sessions. Given that patterns of variability could differ depending on the relative contribution of initial planning errors (which should be most evident early in the movement) vs execution and feedback-related errors, we compared these patterns between spatial locations of the hand at early (peak acceleration) and late (movement endpoint) kinematic landmarks.

II. Methods

A. Experimental Subjects

Two adult male rhesus monkeys (*Macaca mulatta*) were trained for this study. Neither animal had previously been exposed to VR environments. The welfare of the animals conformed to guidelines from the U.S. Public Health Service Policy on Humane Care and Use of Laboratory Animals (Public Law 99-158) and the Guide for the Care and Use of Laboratory Animals (National Academy Press, 1996), and all experimental procedures were approved by the Arizona State University Institutional Animal Care and Use Committee.

B. Motion Capture (mocap) Animation

The VR environment and mocap apparatus have been described in detail elsewhere [9]. Briefly, a marker-based optical mocap system (Motion Analysis Corp., Santa Rosa, CA) was used to record kinematic data of the monkeys' right arm movements. Reflective spherical markers (12.5 mm diameter) were positioned on the shoulder, bicep, elbow, forearm, and wrist via custom-made sleeve fitted to the animals' right arms.

*Research supported by National Science Foundation Division of Integrative Organismal Systems Award 1558151.

P. VanGilder, K. Phataraphruk, and C. A. Buneo are with the School of Biological and Health Systems Engineering, Arizona State University, Tempe, AZ 85287 USA (phone: 480-727-0841; fax: 480-727-7624; e-mail: cbuneo@asu.edu).

Ten cameras were positioned throughout the experimental room at various locations and oriented to create a 1150 x 700 x 300 mm (width, depth, height) capture volume surrounding the monkeys' workspace. Camera locations were chosen to optimize spatial precision and ensure at least three cameras could continually detect each marker regardless of limb movement or orientation within the workspace.

Before recording, the motion-capture editing software *Cortex 2016* identified the markers and their relative positions, saving them to a biomechanical model template of the animals' arms. Realistic avatars identical to each monkey's right arm were constructed from reference photos (Baltu Technologies, Inc., Mesa, AZ) using 3D graphics software (Blender Foundation., Amsterdam, Netherlands). The avatars were animated and driven using skeleton models constructed in *Maya* (Autodesk, Inc., San Rafael, CA). These models defined which joints drove translations and rotations of their corresponding dependent joints for realistic kinematic movements. The skeleton models were bound to mesh and texture layers of the avatar, enabling the joints to modify the appearance of the avatar (e.g. deformation) during animation. These skeleton models were then merged with the monkeys' biomechanical model templates from *Cortex* so that the mocap data animated the avatars' movements.

The *Calcium Solver* engine in *Cortex* used the joint parameters and marker data to calculate the kinematics of the skeleton models. During real-time mocap, *Cortex* sent this kinematic data via SDK2 streaming to a Unity game engine (Unity Software Inc., San Francisco CA), which rendered the avatar within the VR environment.

C. Experimental Paradigm

The animals were seated at a table facing a display mirror oriented at an angle of approximately 45 degrees, which blocked vision of their real arms. The VR environment and virtual arm avatars were displayed on a 3D monitor that was placed above the table and projected onto the mirror. On a given trial, reaches were performed from a starting position located 17 cm in front of the animals on the body midline to a sequence of two visually cued target locations. Four targets were used; two were located 10 cm directly left and right of the starting position and two additional targets were placed at the same lateral positions but 10 cm closer to the animals. Spherical behavior windows surrounded the start position (~3.5cm radius) and reach targets (~4.7cm radius), and the animals were required to accurately reach and maintain positions within these windows for a successful trial.

Each trial began with a 1200-1700ms holding period at the starting position, followed by the presentation of an initial randomly selected target, which cued the animals to reach. After the target was acquired, another holding period of 1200-1700ms commenced, followed by the presentation of a 2nd randomly selected target. Blocks of trials comprised 15 successful reaches to each pseudo-randomly interleaved initial target.

Concurrent tactile feedback was provided by round plastic disks that were similar in size, shape, and color to the VR targets and which were placed on the table at the target positions. A custom LabVIEW program (National Instruments, Austin TX) controlled the entire task including randomizing trials, timing of target onset and offset, monitoring of task performance, and recording of positional data for post-hoc analyses.

D. Data Analysis

For this report, behavioral analyses focused on the first reach in the two-movement sequence. Spatial coordinates (x,y,z) of the hand for each trial were sampled at 125Hz and filtered with a second order Butterworth filter (cutoff frequency of 12.5Hz). Tangential velocity and acceleration were computed by differentiating the positional data. Movement onset/offset were defined as the points where tangential velocity crossed a threshold of 10% of max velocity. Positional data for each trial were visually inspected for verification.

Spatial variability in reach trajectories was quantified at two kinematic landmarks: the point of peak acceleration and the reach endpoint. For a given experimental session, overall variability was quantified by computing the 95% confidence ellipsoids for the distributions of hand positions associated with each kinematic landmark. To identify the axis in space along which variability was maximal, principal components analysis (PCA) was applied to each distribution of hand positions. The orientation of the first eigenvector was then parameterized in terms of its azimuth (orientation relative to the x-axis within the horizontal plane) and elevation (orientation out of horizontal plane). These measures were computed for five experimental sessions for each monkey, conducted over the course of approximately two weeks.

III. Results

A. Reaching Behavior

Figure 1 shows top-down views of the reach paths from the starting position to each target location for both monkeys. Data for all trials and experimental sessions are shown. Although the data presented here have been projected onto the horizontal plane containing the targets, these paths were constructed from the full 3D trajectories, and all subsequent analyses are on the 3D data. Start (square) and target locations (diamonds) are superimposed on the figure, with Target 1 being bottom left (blue paths) and the others numbered counterclockwise.

The reach paths appear slightly offset from the start/target locations due to the placement of the motion capture marker on the wrist of the animals. There were notable differences in the paths between Monkey P and monkey Q, which reflect different reaching strategies. In addition to showing greater variability, paths from monkey P appear to show greater evidence of terminal corrections. In contrast, Monkey Q's hand paths showed little evidence of such adjustments.

The 95% confidence ellipsoids for hand position are displayed in Fig. 2 for peak acceleration (top) and reach

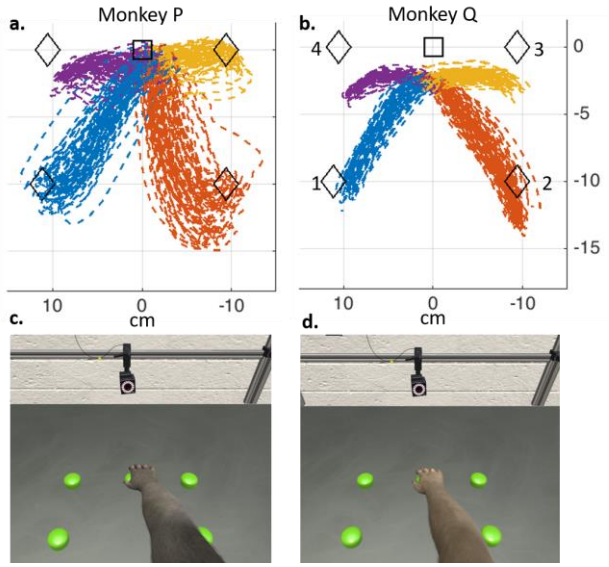

Figure 1. Top-down view of reach paths for all trials across all experimental sessions for Monkey P (a) and Monkey Q (b) The square shape in each figure is the starting position and the diamond shapes are the four reach targets. Targets are numbered starting with bottom left (blue) and proceeding counterclockwise. c-d: Virtual target arrangement and avatar arms for Monkeys P and Q.

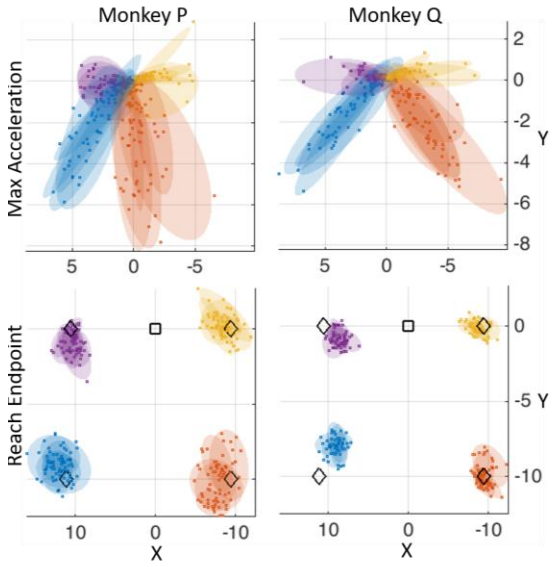

Figure 2. Minimum volume ellipsoids for spatial position of the hand at two time points during the reach: peak acceleration (top) and reach endpoint (bottom). The 95% confidence ellipsoids for each of five recording sessions are overlaid on each other. Colored points are the spatial position (x,y,z) of the hand for each trial. The start and target locations are indicated using the same conventions as Figure 1.

endpoint (bottom). For both monkeys, ellipsoids at peak acceleration exhibited a highly elongated shape, with the primary axis generally aligning with the initial movement direction.

In contrast, ellipsoids at the endpoint were more isotropic, and the directions of the primary axes appeared more variable. With regard to overall magnitude, ellipsoid volumes were found to be considerably larger at peak acceleration (Monkey P: M=21.75, SD=10.86 cm^3; Monkey Q:M=9.9, SD= 3.90 cm^3) than at the reach endpoint (Monkey P: M=4.65, SD=2.94 cm^3; Monkey Q: M:1.25, SD=0.46 cm^3). To directly compare differences in orientation across days, we overlaid the 1st eigenvectors derived from PCA for reach endpoint and peak acceleration on unit circles, depicting the orientations of the distributions of hand positions within the horizontal plane. Figure 3 shows the endpoint (solid lines) and peak acceleration (dashed lines) eigenvectors for Monkey P. Only eigenvectors that accounted for at least 60% of the variance on a given day are shown. Note that eigenvectors were computed in 3D space but are presented from a top-down perspective; thus, eigenvectors that are the length of the circle diameter correspond to distributions of hand positions that were largely confined to the horizontal (target orientation) plane.

Ellipsoid orientations varied with target location for both kinematic landmarks. For a given target, orientations across days were closely aligned at peak acceleration (Circular SD= 3.07°, 9.94°, 5.61°, and 4.42° for targets 1-4, respectively). At the endpoint however, variability in orientation across days was larger and more target dependent. For example, regarding the target dependence, orientations were much more variable for reaches toward Targets 1 and 2, despite the fact that corresponding orientations at peak acceleration were highly similar. The overall larger target dependent variability in orientation was evident in the circular standards deviations, which were 42.93°, 27.85°, 8.53°, and 21.68° for Targets 1-4, respectively.

We found similar trends for Monkey Q, as seen in Fig. 4. Here again orientations exhibited directional dependence, though not to the same degree as for Monkey P. Orientations were again very consistent across days within a given target, with circular standard deviations of 4.50°, 4.19°, 7.75°, and 5.92° for Targets 1-4, respectively. Monkey Q's endpoint orientations were more variable than those at peak acceleration for Targets 1 and 4 (circular SD=12.26° and 8.18°, respectively) but were less variable for Targets 2 and 3 (circular SD= 1.76°, 2.62° respectively). Eigenvector orientations for reaches to Target 2 were highly similar across days for both peak acceleration and reach endpoint, with only a single experimental session showing a deviation from this trend, and in that case the first principal component explained less than 60% of the variance.

Figure 5 shows a scatter plot relating the orientations (i.e., azimuth angles) of the first eigenvectors at peak acceleration to the corresponding eigenvectors at the endpoint. For most targets, there was no clear relationship between the eigenvector orientations at peak acceleration and movement endpoint. Orientations for peak acceleration (y-axis) were generally consistent within targets for both animals. However, variability in the corresponding endpoint orientations (x-axis) was larger and more animal-dependent, particularly for Targets 1 and 2. In contrast, orientations for Target 3 were highly consistent for both animals.

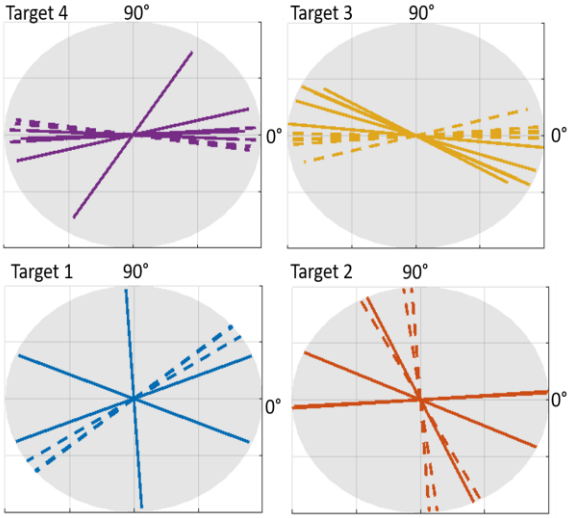

Figure 3. Eigenvector orientations for each target for monkey P for reach endpoint (solid lines) and peak acceleration (dashed lines). Figures are unit circles depicting angle of eigenvector relative to x-axis. Target numbering and color convention as in Figure 1.

IV. Conclusion

Here we investigated the variability of reaching movements performed in VR across multiple experimental sessions in two monkeys, focusing on the coordinates (x,y,z) of the hand at two kinematic landmarks: peak acceleration and reach endpoint. Variability in hand position was found to be generally larger at peak acceleration than at the reach endpoint but was relatively consistent across days and within animals. Although highly elongated in shape, hand position distributions at peak acceleration were also largely consistent in orientation both within and between animals. In contrast, distributions at the reach endpoint were smaller, more isotropic, and more variable and idiosyncratic in orientation. The observation that hand position distributions at peak acceleration were elongated along the movement direction suggests larger errors in planning reach extent vs. reach direction, consistent with previous results in human subjects [10]. That hand position distributions were smaller and less

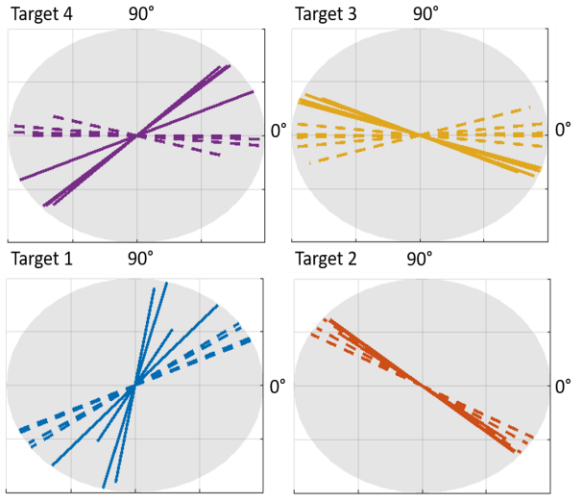

Figure 4. Eigenvector orientations for each target for monkey Q. Figure conventions as in Fig. 3.

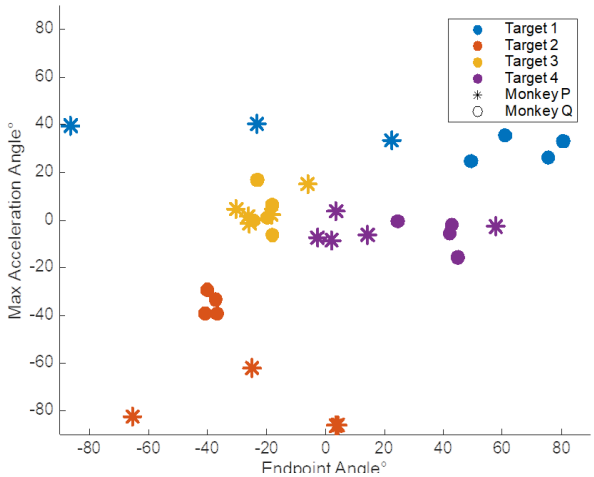

Figure 5. Comparison of eigenvector orientations (i.e. azimuth angles) for hand positions at peak acceleration and reach endpoint.

elongated at the reach endpoint implies that patterns of endpoint variability reflect processes other than planning noise. Execution errors as well as on-line corrective processes appear to contribute more strongly to variability at the endpoint than in the initial stages of movement, and the relative roles of each factor may vary over multiple days or between animals. The results therefore highlight the benefits of using early kinematic landmarks such as peak acceleration for quantifying movement variability in reaching studies involving animals.

References

[1] A. A. Faisal, L. P. J. Selen, and D. M. Wolpert, "Noise in the nervous system," *Nat. Rev. Neurosci.*, vol. 9, no. 4, pp. 292–303, 2008.

[2] C. A. Buneo, J. Boline, J. F. Soechting, and R. E. Poppele, "On the form of the internal model for reaching," *Exp. Brain Res.*, vol. 104, no. 3, pp. 467–479, 1995.

[3] M. M. Churchland, A. Afshar, and K. V. Shenoy, "A Central Source of Movement Variability," *Neuron*, vol. 52, no. 6, pp. 1085–1096, Dec. 2006.

[4] G. A. Apker and C. A. Buneo, "Contribution of execution noise to arm movement variability in three-dimensional space," *J. Neurophysiol.*, vol. 107, no. 1, pp. 90–102, 2012.

[5] M. O. Ernst and H. H. Bülthoff, "Merging the senses into a robust percept," *Trends Cogn. Sci.*, vol. 8, no. 4, pp. 162–169, 2004.

[6] D. C. Knill and A. Pouget, "The Bayesian brain: The role of uncertainty in neural coding and computation," *Trends Neurosci.*, vol. 27, no. 12, pp. 712–719, 2004.

[7] K. P. Körding and D. M. Wolpert, "Bayesian integration in sensorimotor learning," *Nature*, vol. 427, no. 6971, pp. 244–247, Jan. 2004.

[8] D. E. Angelaki, Y. Gu, and G. C. DeAngelis, "Multisensory integration: psychophysics, neurophysiology, and computation," *Curr. Opin. Neurobiol.*, vol. 19, no. 4, pp. 452–458, 2009.

[9] K. Phataraphruk, P. S. VanGilder, and C. A. Buneo, "Virtual Reality Platform for Systematic Investigation of Multisensory Integration and Training of Closed-Loop Prosthetic Control," in *2020 42nd Annual International Conference of the IEEE Engineering in Medicine & Biology Society (EMBC)*, 2020, vol. 2020-July, pp. 2942–2945.

[10] J. Messier and J. F. Kalaska, "Comparison of variability of initial kinematics and endpoints of reaching movements," *Exp. Brain Res.*, vol. 125, no. 2, pp. 139–152, 1999.